



# Thermal decoherence and laser cooling of Kerr microresonator solitons

Tara E. Drake<sup>1,2,3,4</sup>, Jordan R. Stone<sup>1,2,4</sup>, Travis C. Briles<sup>1,2</sup> and Scott B. Papp<sup>1,2</sup>

**Thermal noise is ubiquitous in microscopic systems and high-precision measurements. The control of thermal noise would reveal quantum regimes<sup>1</sup> and enable fundamental physics searches<sup>2</sup>. Recently, nonlinearity in microresonators has enabled laser devices such as Kerr microresonator soliton frequency combs<sup>3</sup>. Soliton microcombs explore nonlinear dynamics and enable optical synthesizers<sup>4</sup>, optical clockwork<sup>5</sup> and data communications systems<sup>6</sup>. Here, we explore how thermal noise leads to the fundamental decoherence of microcombs. We show that a particle-like soliton, which is an ensemble of comb modes, is closely coupled to the thermal fluctuations of its silicon-chip-based resonator. The microcomb modal linewidth is thus thermally broadened, and we characterize these thermal-noise correlations through a soliton effective temperature. Moreover, we demonstrate that passive laser cooling reduces soliton thermal decoherence to far below the ambient-temperature limit. We implement laser cooling by photothermal forcing, and we observe cooling of the frequency comb modes to 84 K. Our work illuminates inherent connections between nonlinear photonics and microscopic fluctuations.**

Thermal energy is constantly being exchanged between matter in thermal equilibrium, leading to fluctuations in physical systems. Specifically, in a homogeneous medium at temperature  $T$  the thermal fluctuations of an observable  $X$  vary by

$$\langle \delta X^2 \rangle = \eta_X^2 \frac{k_B T^2}{\rho C V}, \quad (1)$$

where  $\eta_X = dX/dT$  is the thermal coupling coefficient,  $k_B$  is the Boltzmann constant,  $\rho$  is the mass density,  $C$  is the specific heat, and  $V$  is the volume<sup>7</sup> (see also Methods). Hence, temperature-dependent observables are stochastic variables with measurement uncertainties imposed by the environment. This fundamental limit has been of interest in low-noise optical metrology, where the measurement sensitivity is set by the thermal fluctuations of a cavity or interferometer<sup>8,9</sup>. Thermal-noise-mitigated optical resonators have facilitated some of the most precise measurements and are directly applied in gravitational-wave detection<sup>10</sup> and optical-atomic timekeeping<sup>11</sup>. Furthermore, some systems provide a route to lower temperature through laser cooling, which has revolutionized atomic physics by allowing atoms to be trapped, manipulated and probed for long periods of time<sup>12</sup>. In cavity optomechanics<sup>13</sup>, photothermal and radiation-pressure forces are used to cool mechanical oscillators towards the quantum regime<sup>14,15</sup>. Practical laser cooling of bulk solids through anti-Stokes fluorescence has also been demonstrated<sup>16</sup>.

Microresonators are an important integrated-photonics technology<sup>17</sup> in which both thermal noise and optical nonlinearity play

a large part. However, the intersection of these regimes remains largely unexplored. Thermo-mechanical (thermal expansion) and thermorefractive (temperature-dependent refractive index) effects contribute to the stochastic fluctuations of microresonator modes<sup>18</sup>, with microresonator geometry and thermal coefficients defining the practical impact of thermal noise. Additionally, the index of refraction of Kerr microresonators depends on the intensity of the continuous-wave laser pump, enabling the generation of new frequencies and exotic patterns in the intracavity electromagnetic field. Of particular interest are Kerr soliton frequency combs<sup>3</sup>, which are stationary eigensolutions of the Kerr microresonator field. Various aspects of soliton microcombs have been explored, including their threshold properties<sup>19</sup>, breathing excitations<sup>20</sup>, and crystallization<sup>21</sup>. Thermorefractive-noise models can predict phase noise in soliton microcombs, especially the inverse scaling with mode volume, but there have been no quantitative predictions or experiments.

Here, we use ultraprecise optical-frequency metrology to uncover the thermodynamic behaviour of Kerr solitons. We report that thermal noise imposes fundamental decoherence on the repetition frequency ( $f_{\text{rep}}$ ) of a soliton circulating in a microscopic resonator. Therefore, thermal noise defines the measurement uncertainty of the optical-mode frequencies

$$\nu_n = n f_{\text{rep}} + f_{\text{ceo}} \quad (2)$$

that comprise the soliton microcomb, where  $f_{\text{ceo}}$  is the carrier-envelope-offset frequency<sup>22</sup> and  $n$  is the mode number. We use a silicon nitride ( $\text{Si}_3\text{N}_4$ , hereafter SiN) ring resonator to create an octave-spanning microcomb, and  $f$ - $2f$  self-referencing enables precision-enhanced measurements of  $n f_{\text{rep}}$  by the frequency relationship of equation (2). These results show that the particle-like soliton pulse train—the frequency comb itself—is governed by the ambient temperature. However, the soliton can also be influenced by external fields coupled to the microresonator. We report soliton laser cooling through passive microresonator forcing, which reduces the soliton microcomb's effective temperature to 84 K. We apply the dissipation needed to achieve laser cooling with the photothermal effect of a separate continuous-wave laser. Since there is a direct and conservative coupling between the resonator and the soliton, cooling the effective temperature of one produces a proportional change to the temperature of the other. We observe cooling directly through a reduction in the soliton microcomb's optical linewidth from 2.2 MHz at ambient temperature to 280 kHz at 84 K.

Figure 1a–c illustrates the concept of our experiments and our key observations of thermal decoherence in soliton microcombs. Our photonic device is a planar, waveguide-coupled SiN ring resonator; see Fig. 1a. By pumping mode  $m$  of the resonator at frequency

<sup>1</sup>Time and Frequency Division, National Institute of Standards and Technology, Boulder, CO, USA. <sup>2</sup>Department of Physics, University of Colorado, Boulder, CO, USA. <sup>3</sup>Present address: Center for High Technology Materials and Department of Physics and Astronomy, University of New Mexico, Albuquerque, NM, USA. <sup>4</sup>These authors contributed equally: Tara E. Drake, Jordan R. Stone. ✉e-mail: [scott.papp@nist.gov](mailto:scott.papp@nist.gov)

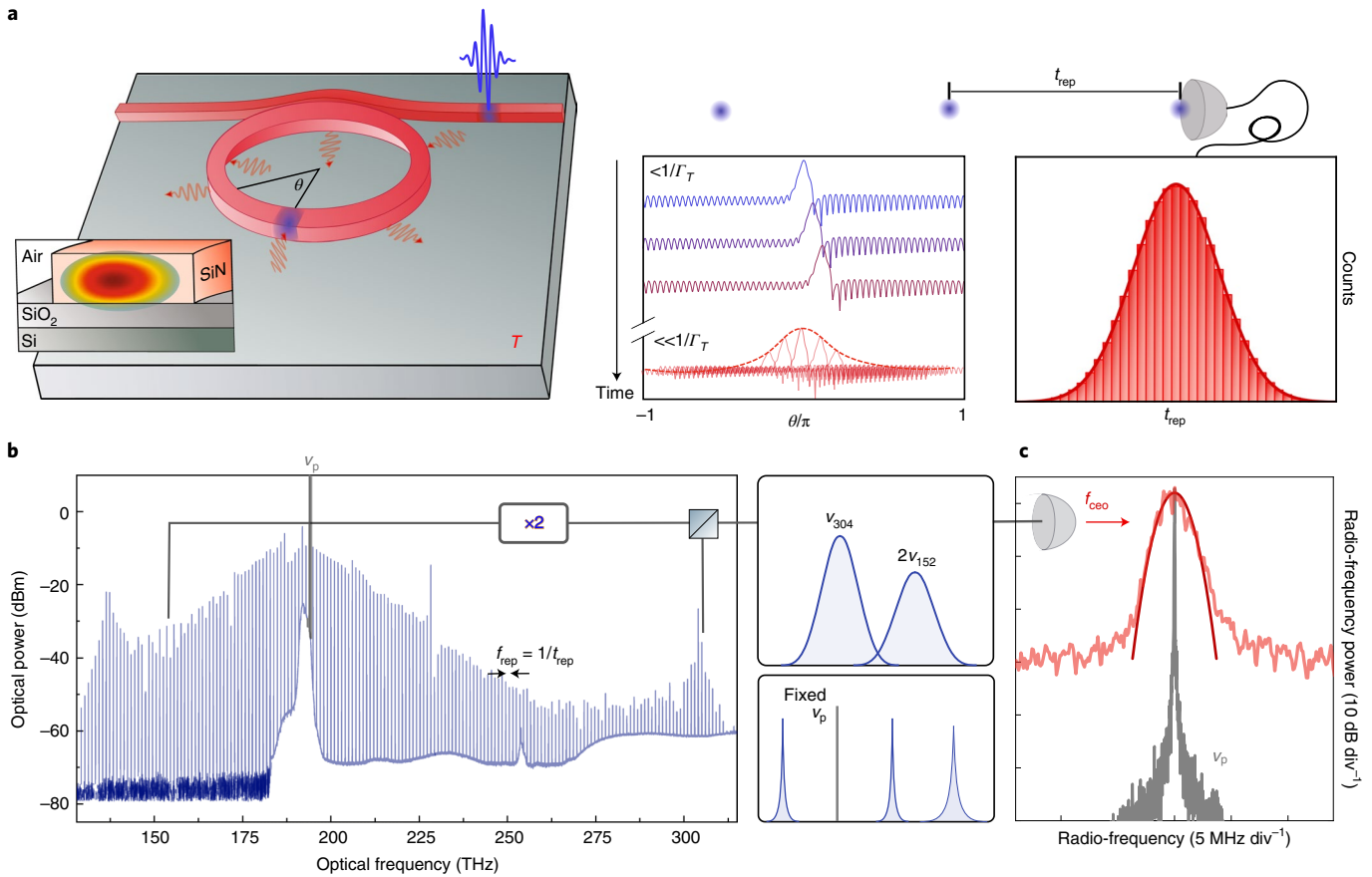


**Fig. 1 | Concept of soliton thermal decoherence.** **a**, Thermal noise induces refractive-index fluctuations that couple to the soliton group velocity. The soliton parameters—including its angular position  $\theta$  (in a frame moving at the average soliton group velocity; middle panel),  $t_{\text{rep}}$ ,  $f_{\text{rep}}$  and  $f_{\text{ceo}}$ —fluctuate due to thermal noise and, after many round trips, must be represented by stochastic ensembles subject to equation (1). Right panel: histogram counts of roundtrip-time measurements. This decoherence occurs on a timescale set by the resonator thermal relaxation rate,  $\Gamma_T$ . **b**, Left panel: the soliton microcomb optical spectrum. Right bottom panel: coherent multiplication of  $f_{\text{rep}}$  fluctuations underlie the thermal broadening of comb modes. Right top panel: conceptual optical spectrum of comb lines used for self referencing. These lines are spectrally broad, because  $f_{\text{rep}}$  fluctuations are amplified in  $f_{\text{ceo}}$  by the factor  $m$  in equation (4). (Our depiction of comb-line broadening is exaggerated for conceptual clarity.) **c**, Measured  $f_{\text{ceo}}$  lineshape (red data). Our theoretical model (dark red line) of the  $f_{\text{ceo}}$  lineshape at  $T = 300$  K overlays the data. For comparison, we show the optical lineshape of the pump laser (grey). Inset: depiction of photodetector for the carrier-envelope-offset frequency.

$\nu_m \approx c/1,546$  nm with a tunable, amplified continuous-wave laser, we generate a soliton with repetition frequency  $f_{\text{rep}} \approx 1.01$  THz. Our experiments and analysis show that  $f_{\text{rep}}$  of the emitted soliton pulse train is influenced by thermal noise through the thermorefractive effect. Here the refractive index  $n(T)$  is a thermodynamic variable subject to equation (1)<sup>18,23</sup>, and this links soliton fluctuations to the resonator temperature  $T$  (regarding thermal equilibrium and equation (1), see the Methods). We consider the thermorefractive frequency fluctuations of  $\delta\nu_m$ , using the Langevin equation

$$\frac{d(\delta\nu_m)}{dt} = -\Gamma_T \delta\nu_m + \zeta(t), \quad (3)$$

where  $\Gamma_T$  is the thermal relaxation rate,  $\zeta(t)$  is a noise source defined by its autocorrelation,  $\langle \zeta(t)\zeta(t + \tau) \rangle = \eta_m^2 \frac{2\Gamma_T k_B T^2}{\rho C V} \delta(\tau)$ ,  $\eta_m = \frac{d\nu_m}{dT}$  is the thermal tuning of the pumped resonator mode (measured for our microresonator as  $-2.4$  GHz K<sup>-1</sup>) and  $\delta(\tau)$  is the Dirac delta function<sup>24</sup>. In equation (3), we do not explicitly include heating due to optical absorption of the red-detuned pump laser, but we note that its practical effect is to increase the resonator mode temperature from  $T \approx 293$  K to  $T \approx 300$  K. Solitons are periodically outcoupled from the resonator at period  $t_{\text{rep}} = 1/f_{\text{rep}}$  and with stochastic noise  $\delta t_{\text{rep}}$  that is related to the pulse train timing jitter.

Hence, repeated measurements of  $t_{\text{rep}}$  at time intervals  $\tau$  become uncorrelated for  $\tau \gg 1/\Gamma_T$ , yielding a distribution of measurement results (Fig. 1a) according to  $\langle \delta f_{\text{rep}}^2 \rangle = \eta_{\text{rep}}^2 \frac{k_B T^2}{\rho C V}$ , where  $\eta_{\text{rep}}$  is the coupling coefficient for thermal noise and  $f_{\text{rep}}$ ; we have measured  $\eta_{\text{rep}} = -2.4$  MHz K<sup>-1</sup> through the characterization reported in Fig. 2.

We detect  $f_{\text{ceo}}$  and perform systematic experiments to characterize it. With soliton microcombs, the mode-frequency relationship of equation (2) yields the coherent signal-frequency relationship

$$f_{\text{ceo}} = \nu_p - m f_{\text{rep}}, \quad (4)$$

where  $\nu_p$  is the pump-laser frequency. As a result, thermal fluctuations are phase-coherently multiplied (Fig. 1b) according to  $\delta f_{\text{ceo}} = -m \times \delta f_{\text{rep}}$ . The red data in Fig. 1c shows the  $f_{\text{ceo}}$  optical lineshape, which is the  $f-2f$  optical-heterodyne beat note. Indeed, the measured full-width at half-maximum (FWHM) is  $\kappa_{\text{ceo}} = 2.2$  MHz, and this linewidth is substantially larger than the contribution from the pump laser, which is shown by the grey trace in Fig. 1c. We characterize the pump laser linewidth via optical heterodyne with a narrower linewidth reference. We model the thermal-noise-limited  $f_{\text{ceo}}$

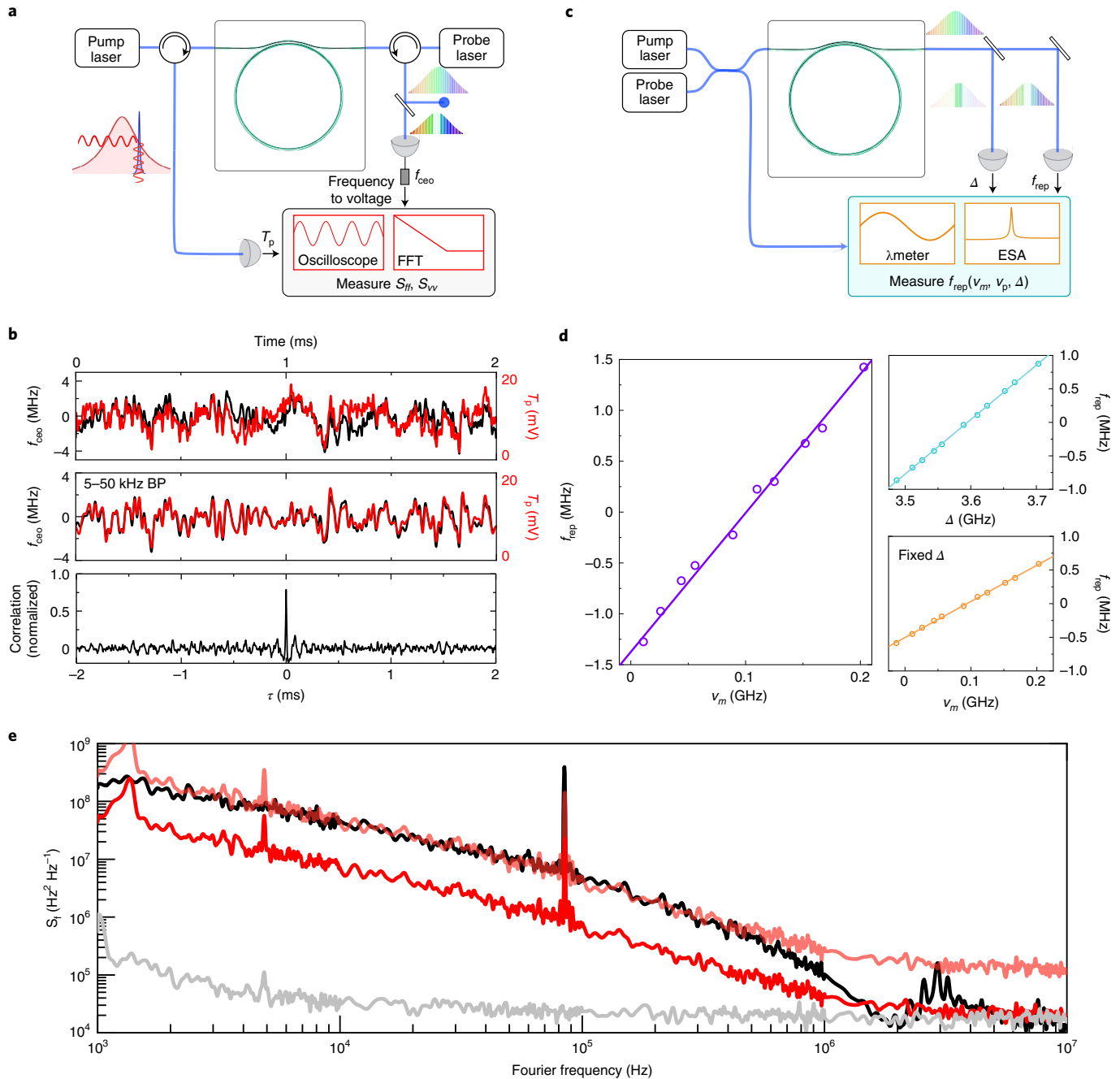


**Fig. 2 | Soliton thermal-noise coupling.** **a**, Schematic for synchronous measurement of  $\nu_m$  and  $f_{\text{ceo}}$  fluctuations. **b**, Top and middle panels: real-time measurements of probe-laser transmission and  $f_{\text{ceo}}$ . A digital bandpass filter (BP) from 5 kHz to 50 kHz is applied in the middle panel. Bottom panel: normalized correlation of the probe transmission and  $f_{\text{ceo}}$ . The peak at  $\tau = 0$  indicates strong thermal-noise correlations. **c**, Schematic for calibrating the thermal-coupling coefficients.  $\lambda$ meter, wavemeter; ESA, electronic spectrum analyser. **d**,  $f_{\text{rep}}$  measurements. Left panel:  $f_{\text{rep}}$  versus  $\nu_m$ . Multiplication of this slope by  $\eta_m$  yields  $\eta_{\text{rep}}$ . Right panels: from the description in the Methods, we isolate the two partial derivatives on the right side of equation (6). In the top graph,  $\nu_m$  is fixed, whereas in the bottom graph,  $\Delta$  is fixed. The slopes of these two lines sum to the slope of the purple line in the left panel. Here we have shifted  $\nu_m$  to the displayed range. **e**, Frequency-noise power-spectral densities of  $f_{\text{ceo}}$  ( $S_{ff}$ , black trace),  $\nu_m$  ( $S_{\nu\nu}$ , red trace), and inferred  $S_{ff}$  from thermal noise and coupling coefficient (pale red trace), and measurement noise floor (grey trace).

lineshape (red line in Fig. 1c) based on the power-spectral density of  $f_{\text{ceo}}$  fluctuations, which we label  $S_{ff}$  and  $\langle \delta f_{\text{ceo}}^2 \rangle = m^2 \langle \delta f_{\text{rep}}^2 \rangle$ . Our model predicts a Gaussian lineshape with

$$\kappa_{\text{ceo}} = \sqrt{8 \ln(2)} m^2 \eta_{\text{rep}}^2 \frac{k_B T^2}{\rho C V}, \quad (5)$$

which evaluates to 2.3 MHz at  $T=300$  K; see the Methods. Our observations highlight the relatively large disparity in linewidth contributions from thermal noise and the pump laser.

Understanding the thermal-noise coupling coefficient  $\eta_{\text{rep}} \equiv df_{\text{rep}}/dT$  is critical; we therefore now explain our modelling and measurements of  $\eta_{\text{rep}}$ . In essence, we seek to define the coupling  $S_{ff}(\omega) = m^2 \eta_{\text{rep}}^2 S_{TT}(\omega) = m^2 \eta_{\text{rep}}^2 S_{\nu\nu}(\omega)/\eta_m^2$ , where  $\omega$  is the angular Fourier frequency, and  $S_{TT}$  and  $S_{\nu\nu}$  are the power-spectral

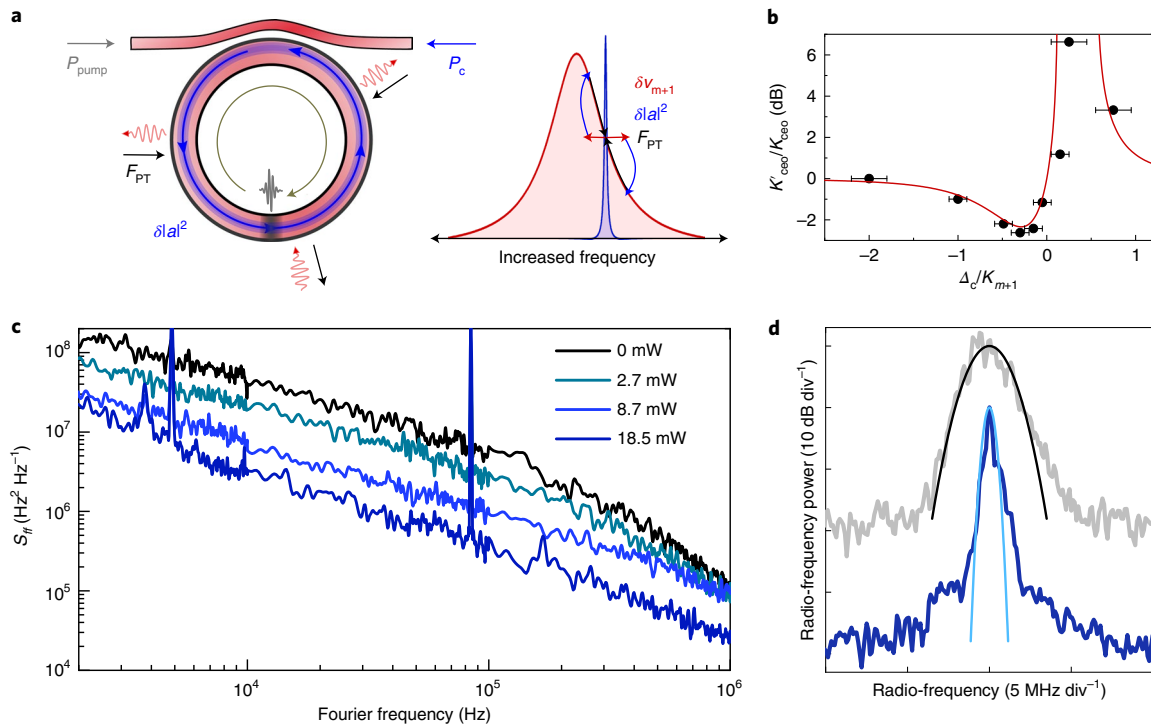


**Fig. 3 | Soliton laser cooling.** **a**, Conceptual illustration of the photothermal forcing,  $F_{PT}$ , used to dynamically maintain  $\Delta_c$ . We tune the cooling laser approximately one-half linewidth higher frequency than  $\nu_{m+1}$ . Thermorefractive noise causes a fluctuation in the intracavity energy,  $|a|^2$ , which the cooling laser passively counters. **b**, Measured  $f_{ceo}$  linewidth versus  $\Delta_c$  for  $P_c = 5$  mW. The linewidth model shown by the red line is based on equation (5) and the photothermal cooling effect  $\Gamma_T'/\Gamma_T$ . Error bars indicate the systematic uncertainty of detuning. **c**,  $S_{ff}(\omega)$  for  $P_c = 0$  mW, 2.7 mW, 8.7 mW and 18.5 mW. **d**, Measured  $f_{ceo}$  power spectrum without cooling (black) and for  $P_c = 18.5$  mW (blue). The data are compared to the model from equation (5).

densities of the resonator-mode thermal noise and resonator-mode frequency noise, respectively. We assume  $f_{rep} = \frac{1}{2\pi} \left( D_1 + \Omega(\Delta) \frac{D_2}{D_1} \right)$ , where  $D_1/2\pi$  is the microresonator free spectral range,  $D_2/2\pi$  is the second-order coefficient of a series expansion around  $\nu_m$  that calculates the mode frequencies, and  $\Omega(\Delta)$  is a frequency shift in the soliton carrier wave that depends on the pump-resonator detuning,  $\Delta = \nu_m - \nu_p$  (ref. 25). Since temperature changes induce shifts in  $\nu_m$  and  $\Delta$ , we decompose  $\eta_{rep}$  as

$$\eta_{rep} = \frac{df_{rep}}{d\nu_m} \frac{d\nu_m}{dT} = \left( \frac{\partial f_{rep}}{\partial \nu_m} + \frac{\partial f_{rep}}{\partial \Delta} \right) \eta_m. \quad (6)$$

Equation (6) is a key result that reveals the coupling of  $f_{rep}$  to temperature owing to the microresonator dispersion and soliton frequency shift,  $\Omega(\Delta)$ . In Fig. 2 we test this prediction and explore other properties of  $\eta_{rep}$ . First, we measure correlations of  $\nu_m$  and  $f_{ceo}$  by the configuration in Fig. 2a; see Methods for more details. To measure  $\nu_m$  fluctuations, we use a probe laser directed in the reverse direction to that of the pump laser and blue-detuned from  $\nu_{m+1}$  by a half-linewidth. We use the  $\nu_{m+1}$  mode to filter the residual pump light from the measurement, and we photodetect the probe laser intensity noise that is converted from  $\nu_{m+1}$  noise. In addition, we downconvert the  $f_{ceo}$  microwave signal to a baseband frequency and record it by use of an analog frequency-to-voltage circuit. With an oscilloscope, we simultaneously detect these fluctuating signals, which are presented in Fig. 2b after processing with two digital-filter functions. Their correspondence is clear, resulting in the strong cross-correlation peak shown in Fig. 2b. Moreover, we observe no correlation of  $f_{ceo}$  and the pump-laser noise that obscures the thermal noise at high frequency; see Supplementary Information. These measurements reveal the coherent thermal-noise driving of soliton temporal fluctuations by the ambient environment.

Next we measure  $\eta_{rep}$  and characterize our results with equation (6). To measure  $\eta_{rep}$ , we detect  $f_{rep}$  by electro-optic modulation<sup>3</sup>, which reduces the 1-THz mode spacing to a microwave frequency, and probe  $\nu_m$  with a wavemeter-measured laser; see Fig. 2c. With  $\nu_p$  fixed, we thermally tune  $\nu_m$  and record changes in  $f_{rep}$ ; see Fig. 2d and Methods. From a linear fit to these data we obtain  $df_{rep}/d\nu_m = 13.5(2)$  MHz GHz<sup>-1</sup>; hence  $\eta_{rep} = \frac{df_{rep}}{d\nu_m} \eta_m = -32.4(5)$  MHz K<sup>-1</sup>.

Although this measurement is sufficient to predict soliton thermal noise, it does not reveal the relative contributions of  $\partial f_{rep}/\partial \nu_m$  and  $\partial f_{rep}/\partial \Delta$  in equation (6). In the Methods, we describe measurements designed to isolate these coefficients in the experiment; this calibration procedure yields  $\partial f_{rep}/\partial \nu_m = 5.2$  MHz GHz<sup>-1</sup> and  $\partial f_{rep}/\partial \Delta = 8.3$  MHz GHz<sup>-1</sup>. These measurements are shown in the right panels of Fig. 2d.

In Fig. 2e, we present a frequency-domain analysis of soliton thermal noise. We obtain  $S_{ff}$  (black trace) and  $S_{\nu\nu}$  (red trace) from the analog time-domain  $f_{ceo}$  and probe-laser intensity noise signals, respectively, and we focus on the frequency range from 1 kHz to 1 MHz that is dominated by thermal noise. The  $f_{ceo}$  signal presented to our digitizing FFT analyser contains technical drift and noise, and the soliton thermal noise. Although we have not developed a detailed thermal conduction model of the SiN resonator<sup>26</sup>, the frequency dependence of  $S_{ff}$  and  $S_{\nu\nu}$  are consistent with the 1–2  $\mu$ s measured and predicted principal thermal time constant of our resonator; see Supplementary Information for analysis and comparison with an existing model of thermal conduction. Importantly,  $S_{\nu\nu}$  depends sensitively on device geometry, and the thermal noise associated with our device that is optimized for  $f$ - $2f$  measurements is larger than in other SiN resonators<sup>26</sup>. Using our measurement of  $\eta_{rep}$ , we directly compare the inferred spectrum ( $m^2 \eta_{rep}^2 S_{TT}(\omega)$ ) of  $f_{ceo}$  (pale red trace in Fig. 2e) with our  $f$ - $2f$  measurement of  $f_{ceo}$ .

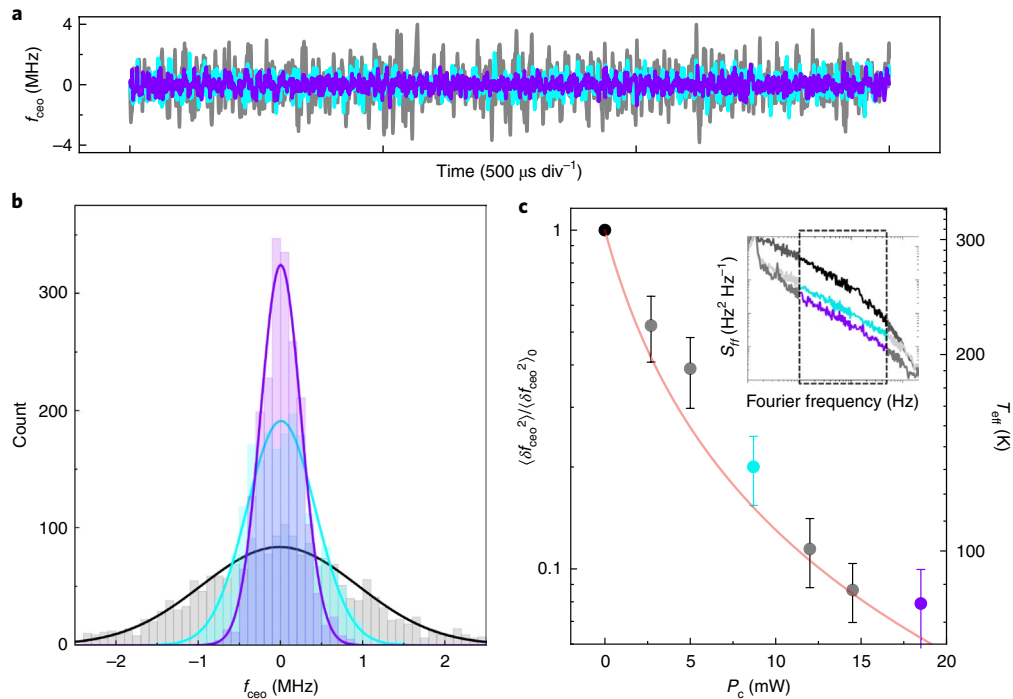


**Fig. 4 | Universal thermal fluctuations.** **a**, Real-time measurement of  $f_{\text{ceo}}(t)$  for no cooling laser (grey) and  $P_c = 8.7$  mW (cyan) and 18.5 mW (violet). **b**, Direct measurement of the  $f_{\text{ceo}}(t)$  distribution, constructed by binning the data in **a**. From these data, we define the effective temperature,  $T_{\text{eff}}$ , using its fundamental connection to  $\langle \delta(f_{\text{ceo}})^2 \rangle$ . **c**,  $T_{\text{eff}}$  versus  $P_c$ . The data from **a** and **b** are indicated by the black, cyan and violet points, and the error bars indicate standard deviation. The expected  $T_{\text{eff}}$  based on  $\Gamma'/\Gamma_T$  and equation (8), is shown in pale red. Inset:  $S_{ff}$  traces from Fig. 3c, with a window corresponding to our applied filter at 10–500 kHz. (See Fig. 3c for units.)

Figure 3 introduces soliton laser cooling, which we implement through a parametric coupling with an auxiliary coherent laser field. Thermal nonlinearity has long been used to reduce relative laser-microresonator technical noises, but it has not been used to address fundamental thermal noise<sup>24</sup>. Specifically, thermo-optic locking is a powerful technique by which bistability leads to dynamic stabilization (de-stabilization) of the laser-resonator system at positive (negative) frequency detuning. Moreover, auxiliary laser schemes to balance microresonator heating in soliton generation have recently been described<sup>27,28</sup>. In these schemes an auxiliary laser is used to pre-heat a resonator, and the laser passively maintains a balance of resonator heating during the transition from a high average power chaotic intracavity waveform to a lower average power soliton stationary state. Our cooling laser gives rise to dynamic photothermal forcing<sup>14</sup>, which counteracts soliton thermal noise for an appropriate setting of the cooling laser ( $\nu_c$ ) frequency detuning  $\Delta_c = \nu_{m+1} - \nu_c$ . Figure 3a shows a schematic of our experiments and an illustration of how resonator-mode thermal fluctuations give rise to intracavity power fluctuations. For negative  $\Delta_c$ , photothermal forcing dynamically maintains  $\Delta_c$ , countering changes in the intracavity power that arise primarily from thermal noise. A positive  $\Delta_c$  amplifies thermal fluctuations. Specifically, we identify the photothermal force,  $F_{\text{PT}} = \alpha_T |a|^2$ , and include it in equation (3); see Methods. Here,  $\alpha_T$  is the thermo-optic heating coefficient, and the cooling-laser intracavity energy  $|a|^2 = \kappa_e P_c / (\Delta_c^2 + (\kappa_{m+1}/2)^2)$  depends on the external coupling rate  $\kappa_e$ , the on-chip cooling laser power  $P_c$ , and the resonator mode linewidth  $\kappa_{m+1}$ . Consequently, laser cooling modifies the thermal relaxation rate to

$$\Gamma' = \Gamma_T + \frac{2 |\alpha_T| \kappa_e \Delta_c}{(\Delta_c^2 + (\kappa_{m+1}/2)^2)^2} P_c, \quad (7)$$

and  $S_{ff}$  is scaled by the ratio  $\Gamma'/\Gamma_T$  (refs<sup>14,24,29</sup>).

We have discovered that the practical effect of soliton laser cooling is  $f_{\text{ceo}}$  frequency-noise reduction within the resonator thermal bandwidth and a correspondingly reduced effective soliton temperature. Therefore, according to our understanding from equation (5), we expect a reduction in the linewidth of  $f_{\text{ceo}}$ , which we denote as  $\kappa'$  for observations with laser cooling applied and  $\kappa_{\text{ceo}}$  without. We directly measure the ratio  $\kappa'/\kappa_{\text{ceo}}$  (Fig. 3b) for several settings of  $\Delta_c$  with fixed  $P_c = 5$  mW, and we observe both a clear reduction and an increase in the  $f_{\text{ceo}}$  linewidth, depending on  $\Delta_c$ . Furthermore, the Langevin model captures this behaviour well, as shown by the red line in Fig. 3b where we predict the  $\Gamma'/\Gamma_T$  reduction in  $S_{ff}$  and the corresponding linewidth based on equation (5) and the Methods. This demonstrates both the utility of our soliton-laser-cooling technique and its connection to external dynamic control of the soliton microcomb.

We explore the  $P_c$ -dependence of soliton laser cooling on  $S_{ff}$ , searching for the conditions that yield the lowest frequency-noise spectrum (Fig. 3c) and the narrowest  $f_{\text{ceo}}$  linewidth (Fig. 3d). In our experiments, for each setting of  $P_c$  we adjust  $\Delta_c$  to maximize laser cooling. With  $P_c = 18.5$  mW power coupled onto the chip, we achieve almost 20 dB of  $S_{ff}$  noise reduction across more than three decades in Fourier frequency. This broadband behaviour is consistent with  $\Gamma_T$  and the relatively low-noise properties of our cooling laser. At still higher settings of  $P_c$ , we do observe some technical complexities of soliton laser cooling; see the Methods. Even constrained to  $P_c \leq 18.5$  mW, soliton laser cooling affects a profound change in the optical lineshape of  $f_{\text{ceo}}$ , as shown in Fig. 3d. Here, the uncooled soliton (grey trace) has an  $f_{\text{ceo}}$  linewidth of 2.2 MHz, according to equation (4), whereas the laser-cooled soliton exhibits a reduced linewidth of 280 kHz and, surprisingly, the signal-to-noise ratio of the  $f_{\text{ceo}}$  lineshape is increased by 10 dB.

Viewing soliton thermal noise and laser cooling through  $S_{ff}$  necessitates a detailed understanding of microresonator materials.

With the complementary set of experiments presented in Fig. 4, we show the universal nature of thermal fluctuations traced back to equation (1) by exploring the ensemble average  $\langle \delta f_{\text{ceo}}^2 \rangle$ . This analysis enables characterization of a thermal-noise-limited soliton by an effective temperature. Specifically, the connection between  $\langle \delta f_{\text{ceo}}^2 \rangle$  and equation (1) defines an effective temperature ( $T_{\text{eff}}$ ) associated with soliton laser cooling, according to

$$T_{\text{eff}} = \sqrt{\frac{\langle \delta f_{\text{ceo}}^2 \rangle \rho C V}{m^2 n_{\text{rep}}^2 k_B}} = T_0 \sqrt{\frac{\langle \delta f_{\text{ceo}}^2 \rangle}{\langle \delta f_{\text{ceo}}^2 \rangle_0}}, \quad (8)$$

where  $T_0$  is the ambient temperature and  $\langle \delta f_{\text{ceo}}^2 \rangle_0$  is the variance in  $f_{\text{ceo}}$  without laser cooling. Hence, a real-time record of  $f_{\text{ceo}}$  contains the full set of information required to understand soliton thermodynamics.

Using the frequency-to-voltage circuit and the digital filter as described previously in Fig. 2c, we have measured  $f_{\text{ceo}}$  fluctuations in real time and with high sensitivity; see Fig. 4a. We verified that our digital filter, which reduces low-Fourier-frequency contributions from pump-laser noise, does not influence our conclusions regarding  $T_{\text{eff}}$ . Without applying laser cooling we record the grey  $f_{\text{ceo}}(t)$  trace that is characterized by a standard deviation of 0.95 MHz. By activating the laser cooling at moderate (maximum) settings of  $P_c$ , we obtain the cyan (violet)  $f_{\text{ceo}}(t)$  trace that shows a decreased standard deviation. We present all three traces as histograms in Fig. 4b, which makes clear that soliton laser cooling reduces  $f_{\text{ceo}}$  noise and increases our measurement precision. We use Gaussian fitting to determine  $\langle \delta f_{\text{ceo}}^2 \rangle$  and hence  $T_{\text{eff}}$  from the histograms. In our experiments, we vary  $P_c$  and record the variance of  $f_{\text{ceo}}$  normalized to the case of  $P_c = 0$ ; see Fig. 4c. We expect a reduction in  $T_{\text{eff}}$  with increasing  $P_c$ , according to equation (8) and the Langevin laser-cooling model for  $\Gamma_T/\Gamma'_T$  that we show (red line) in Fig. 4c. We assess that the laser-cooled soliton effective temperature can reach  $T_{\text{eff}} \approx 84$  K; otherwise immersion of our entire photonic chip in liquid nitrogen might be required.

In summary, we demonstrate strong thermal-noise correlations of the repetition frequency in soliton microcombs that fundamentally limits the precision of optical-frequency measurements. However, passive photothermal laser cooling of the soliton microcomb can mitigate thermal noise, as we observe through a reduced effective temperature, improved coherence and enhanced signal-to-noise ratio in carrier-envelope-offset frequency detection. Our work demonstrates that innovation in integrated photonics will depend on understanding the part that microscopic physics and its control play in nanophotonics.

### Online content

Any methods, additional references, Nature Research reporting summaries, source data, extended data, supplementary information, acknowledgements, peer review information; details of author contributions and competing interests; and statements of data and code availability are available at <https://doi.org/10.1038/s41566-020-0651-8>.

Received: 13 May 2019; Accepted: 15 May 2020;

Published online: 22 June 2020

### References

- Anderson, M. H., Ensher, J. R., Matthews, M. R., Wieman, C. E. & Cornell, E. A. Observation of Bose–Einstein condensation in a dilute atomic vapor. *Science* **269**, 198–201 (1995).

- Parker, R. H., Yu, C., Zhong, W., Estey, B. & Müller, H. Measurement of the fine-structure constant as a test of the standard model. *Science* **360**, 191–195 (2018).
- Kippenberg, T. J., Gaeta, A. L., Lipson, M. & Gorodetsky, M. L. Dissipative Kerr solitons in optical microresonators. *Science* **361**, eaan8083 (2018).
- Spencer, D. T. et al. An optical-frequency synthesizer using integrated photonics. *Nature* **557**, 81–85 (2018).
- Drake, T. E. et al. Terahertz-rate, Kerr-microresonator optical clockwork. *Phys. Rev. X* **9**, 031023 (2019).
- Marin-Palomo, P. et al. Microresonator solitons for massively parallel coherent optical communications. *Nature* **546**, 274–279 (2017).
- Landau, L. D., Lifshitz, E. M. & Pitaevskii, L. in *Statistical Physics Part I* 333–364 (Pergamon Press, 1980).
- Numata, K., Kemery, A. & Camp, J. Thermal-noise limit in the frequency stabilization of lasers with rigid cavities. *Phys. Rev. Lett.* **93**, 250602 (2004).
- Liu, Y. T. & Thorne, K. S. Thermoelastic noise and homogeneous thermal noise in finite sized gravitational-wave test masses. *Phys. Rev. D* **62**, 122002 (2000).
- Abbott, B. P. et al. Observation of gravitational waves from a binary black hole merger. *Phys. Rev. Lett.* **116**, 061102 (2016).
- Ludlow, A. D., Boyd, M. M., Ye, J., Peik, E. & Schmidt, P. O. Optical atomic clocks. *Rev. Mod. Phys.* **87**, 637–701 (2015).
- Phillips, W. D. Nobel lecture: Laser cooling and trapping of neutral atoms. *Rev. Mod. Phys.* **70**, 721–741 (1998).
- Aspelmeyer, M., Kippenberg, T. J. & Marquardt, F. Cavity optomechanics. *Rev. Mod. Phys.* **86**, 1391–1452 (2014).
- Metzger, C. H. & Karrai, K. Cavity cooling of a microlever. *Nature* **432**, 1002–1005 (2004).
- Gigan, S. et al. Self-cooling of a micromirror by radiation pressure. *Nature* **444**, 67–70 (2006).
- Seletskiy, D. V. et al. Laser cooling of solids to cryogenic temperatures. *Nat. Photon.* **4**, 161–164 (2010).
- Moss, D. J., Morandotti, R., Gaeta, A. L. & Lipson, M. New CMOS-compatible platforms based on silicon nitride and Hydex for nonlinear optics. *Nat. Photon.* **7**, 597–607 (2013).
- Matsko, A. B., Savchenkov, A. A., Yu, N. & Maleki, L. Whispering-gallery-mode resonators as frequency references. I. Fundamental limitations. *J. Opt. Soc. Am. B* **24**, 1324–1335 (2007).
- Li, X. et al. Universal isocontours for dissipative Kerr solitons. *Opt. Lett.* **43**, 2567–2570 (2018).
- Bao, C. et al. Observation of Fermi–Pasta–Ulam recurrence induced by breather solitons in an optical microresonator. *Phys. Rev. Lett.* **117**, 163901 (2016).
- Cole, D. C., Lamb, E. S., Del’Haye, P., Diddams, S. A. & Papp, S. B. Soliton crystals in Kerr resonators. *Nat. Photon.* **11**, 671–676 (2017).
- Jones, D. J. et al. Carrier-envelope phase control of femtosecond mode-locked lasers and direct optical frequency synthesis. *Science* **288**, 635–639 (2000).
- Gorodetsky, M. L. & Grudinin, I. S. Fundamental thermal fluctuations in microspheres. *J. Opt. Soc. Am. B* **21**, 697–705 (2004).
- Sun, X., Luo, R., Zhang, X.-C. & Lin, Q. Squeezing the fundamental temperature fluctuations of a high-Q microresonator. *Phys. Rev. A* **95**, 023822 (2017).
- Yi, X. et al. Single-mode dispersive waves and soliton microcomb dynamics. *Nat. Commun.* **8**, 14869 (2017).
- Huang, G. et al. Thermorefractive noise in silicon-nitride microresonators. *Phys. Rev. A* **99**, 061801 (2019).
- Grudinin, I., Lee, H., Chen, T. & Vahala, K. Compensation of thermal nonlinearity effect in optical resonators. *Opt. Express* **19**, 7365–7372 (2011).
- Zhang, S. et al. Sub-milliwatt-level microresonator solitons with extended access range using an auxiliary laser. *Optica* **6**, 206–212 (2019).
- Restrepo, J., Gabelli, J., Ciuti, C. & Favero, I. Classical and quantum theory of photothermal cavity cooling of a mechanical oscillator. *C. R. Phys.* **12**, 860–870 (2011).

**Publisher’s note** Springer Nature remains neutral with regard to jurisdictional claims in published maps and institutional affiliations.

This is a U.S. government work and not under copyright protection in the U.S.; foreign copyright protection may apply 2020

## Methods

**Soliton generation and self-referencing.** We generate Kerr solitons by use of the fast-sweeping method described in Briles et al.<sup>30</sup> and Stone et al.<sup>31</sup>. A pump laser (New Focus Velocity) is modulated in the single-sideband, suppressed-carrier configuration by a voltage-controlled oscillator with 10–20-GHz output frequency. The pump-laser frequency is blue-detuned of  $\nu_m$  and swept red by 10 GHz to a final, red-detuned optical frequency. The frequency sweep initiates modulation instability in the microresonator and subsequently induces its condensation into a Kerr soliton. Optimizing the sweep speed mitigates thermal transients that arise from sudden changes in intracavity power; we find that an approximately 100-ns sweep time is appropriate for our system.

Our chip contains dozens of photonic circuits with which to vary the dispersive-wave peak wavelengths and the resonator's mode structure, which controls  $f_{\text{ceo}}$ . After guiding the soliton microcomb off-chip, we separate the short- and long-wavelength spectral components for  $f$ - $2f$  self-referencing. The modes near 1,965 nm are amplified with thulium-doped fibre<sup>32</sup>, frequency-doubled in a periodically poled lithium niobate waveguide, and recombined with the 982.5-nm comb mode on an avalanche photodiode. Our experiments demonstrate  $f$ - $2f$  measurement of a microcomb without the aid of external broadening<sup>33,34</sup> or auxiliary lasers<sup>30,35</sup>.

Our periodically poled lithium niobate waveguide (Srico) is approximately 3 cm long and temperature-controlled with off-chip heaters. The temperature is adjusted to optimize phase matching, for an on-chip efficiency of 30% per watt. The frequency-doubled comb light and short-wavelength dispersive wave are combined in a 50% coupler and collectively amplified to about 10  $\mu$ W in a semiconductor optical amplifier.

The nature of the experiments reported here require that we keep the soliton conditions identical from day to day. To achieve this, we relied on a wavemeter to give us the pump laser frequency, monitored the intracavity pump power via both a pick-off and continual checks of laser-device coupling, took periodic measurements of pump-laser-resonance detuning via the method shown in Fig. 2c, and controlled the environmental temperature via a thermo-electric-cooler device mount.

**Theory of thermal  $f_{\text{ceo}}$  linewidth.** A relationship exists between  $\kappa_{\text{ceo}}$ ,  $S_{ff}$  and  $T_{\text{eff}}$ , which we analyse using equation (1). We write the FWHM linewidth of an oscillator as  $\kappa = \sqrt{8 \ln(2)A}$ , where  $A$  is the power spectral density of the frequency fluctuations integrated up to the so-called beta line<sup>36</sup>, defined by  $S_{\beta\beta}(\omega) = \omega \times 4 \ln(2) / \pi^3$ . To predict  $\kappa_{\text{ceo}}$  from the system temperature, we first observe that for  $S_{ff}$  at room temperature, the  $f_{\text{ceo}}$  thermal noise is mostly above  $S_{\beta\beta}$ . This corresponds to the Gaussian noise limit. Hence, we connect  $T$  and  $\kappa_{\text{ceo}}$  as follows

$$\frac{1}{2\pi} \int_{-\infty}^{\infty} S_{ff} d\omega = m^2 \eta_{\text{rep}}^2 \frac{k_B T^2}{\rho C V} \approx \frac{\kappa_{\text{ceo}}^2}{8 \ln(2)}, \quad (9)$$

from which we predict a thermal-noise-limited  $\kappa_{\text{ceo}} = \sqrt{8 \ln(2) \times m^2 \eta_{\text{rep}}^2 \frac{k_B T^2}{\rho C V}}$ . This prediction is consistent with known properties of Gaussian noise processes, including the factor  $\sqrt{8 \ln(2)}$  to convert from the standard deviation to FWHM. Using the measured  $\eta_{\text{rep}} = -32.4 \text{ MHz K}^{-1}$ , literature-backed values of  $\rho = 2,600 \text{ kg m}^{-3}$  and  $C = 650 \text{ J kg}^{-1} \text{ K}^{-1}$  (refs. 37,38), and  $V$  in the range  $3\text{--}4 \times 10^{-17} \text{ m}^3$  based on the FWHM of a finite-element mode simulation, we calculate  $\kappa_{\text{ceo}} = 2.3 \text{ MHz}$ , in agreement with the experimental value of 2.2 MHz. The small mode volume  $V$  exacerbates thermal broadening; a recent study performed using devices with larger optical mode volume measured correspondingly lower thermal broadening<sup>26</sup>. (Since we are not able to measure the SiN material properties, we use literature values for the amorphous, stoichiometric SiN low-pressure chemical-vapour deposition films, namely densities from 2,400  $\text{kg m}^{-3}$  to 2,800  $\text{kg m}^{-3}$  and specific heat values of 600  $\text{J kg}^{-1} \text{ K}^{-1}$  to 700  $\text{J kg}^{-1} \text{ K}^{-1}$ , and take for our calculation the mean value of these ranges.) Propagation of the uncertainties in the material parameters and volume gives  $\rho C V = 5.1(9) \times 10^{-11} \text{ J K}^{-1}$ , and  $\kappa_{\text{ceo}} = 2.3(2) \text{ MHz}$ . The uncertainty in  $\eta_{\text{rep}}$  is reported in the main text and does not substantially contribute to the error analysis.

A theoretical  $f_{\text{ceo}}$  power spectrum based on this model is shown in Fig. 1c. To further quantify our results, we integrate  $S_{\nu\nu}$  to obtain  $\langle \delta\nu_m^2 \rangle$ , which, for a thermal-noise-limited microresonator in equilibrium, is defined by equation (1). Here, we integrate over Fourier frequencies between 5 kHz and 1 MHz to avoid pump-laser and measurement-floor contributions, and assess that these frequencies contribute almost all of the thermal noise<sup>26</sup>. From the integration we obtain  $2.5 \times 10^{11} \text{ Hz}^2$ , consistent with the value  $1.5(2) \times 10^{11} \text{ Hz}^2$  obtained from equation (1). This comparison does not take into account contributions from pump-laser noise, our instrument baseline, and uncertainty in measuring power-spectral density. For example, changing the high frequency integration limit to 500 kHz, where we observe a baseline contribution, changes  $\langle \delta\nu_m^2 \rangle$  to  $1.9 \times 10^{11} \text{ Hz}^2$ . Non-equilibrium corrections to equation (1), which are apparently small, may also be appropriate to describe our system fully.

For soliton microcombs, absorption of both the pump laser and frequency-comb light drives the microresonator away from thermal equilibrium; it is therefore critical to justify our use of equation (1), which is exact only in the equilibrium limit. Importantly, our experiments satisfy the conditions of local equilibrium, so that in equation (1) we use the mode-averaged temperature, which is slightly higher than the ambient temperature. This approximation is suitable for our experiments because, as described in the main text, the mode-averaged temperature is near its equilibrium value (the thermal shifts from optical absorption are small). Moreover, the temperature gradient across the microresonator is small<sup>39</sup>, which implies a negligible temperature difference between the optical mode and the surrounding microresonator material. We note that, although these approximations should be valid for most experiments, they should be confirmed on a case-by-case basis. In particular, the temperature shift induced by the soliton should be small, with negligible correlations between it and the total intracavity energy. Importantly, our laser cooling technique relies on strong correlations between thermal fluctuations and the cooling laser intracavity energy. These correlations create a system that is far from equilibrium, even if the microresonator is not heated substantially. Hence, application of equation (1) yields an effective soliton temperature that is cooled with respect to the real system temperature.

In Fig. 3d, we apply our model to the  $f_{\text{ceo}}$  linewidth reduction from laser cooling. For substantial cooling, a non-negligible fraction of  $S_{ff}$  is reduced below  $S_{\beta\beta}$ , resulting in a narrower  $f_{\text{ceo}}$  spectrum than predicted by the model. While the exact discrepancy depends on the form of  $S_{\beta\beta}$ , in our system we experimentally achieve  $\kappa_{\text{ceo}}' = 280 \text{ kHz}$ , compared to about 640 kHz from the model. We have verified the linewidth reduction through a numerical study of  $S_{ff}$ .

**Cross-correlation measurement.** We operate the probe laser blue-detuned from  $\nu_{m+1}$  by slightly less than a half linewidth. At this detuning, frequency fluctuations in either the probe laser or microresonator are converted in a calibrated fashion to the probe-laser intensity. The probe-laser power is set to <1 mW of chip-coupled power to prevent parametric coupling between the probe and microresonator noise. The intrinsic intensity noise and phase noise of the probe laser are measured separately and are verified not to contribute substantially to the signal. Therefore, we conclude that the probe transmission is a reliable measurement of  $\nu_{m+1}$  frequency fluctuations.

To confirm that  $\nu_{m+1}$  frequency fluctuations are not caused by the pump laser, we perform experiments to understand the role of pump laser noise on the microresonator and soliton (Supplementary Information). As a quick test, we systematically increase the pump laser noise and measure changes in the  $f_{\text{ceo}}$  linewidth,  $\kappa_{\text{ceo}}$ . An electronic noise source is used to drive either an acousto-optic modulator (to increase pump laser intensity noise) or the single-sideband modulator (to increase pump laser frequency noise). Even after adding a substantial amount of broadband noise, we observe no change in  $\kappa_{\text{ceo}}$ .

**Measurement of  $\eta_m$ .** Our photonic chip rests on a copper platform whose temperature we control using a thermo-electric circuit. We measure  $\eta_m$  by measuring  $\nu_m$  (using a weak probe laser and wavemeter) against controlled changes in the temperature setpoint. For this measurement, we estimate that changes in the temperature setpoint correspond to equal changes in the average optical mode temperature, and that thermo-optic effects from the weak probe laser are negligible. Our measurement is in good agreement with previous studies of SiN microresonators<sup>40</sup>.

**Calculation of  $f_{\text{rep}}$  tuning coefficients.** The frequency comb repetition rate is determined by the soliton group velocity and microresonator path length as

$$f_{\text{rep}} = c/n_g(\omega_s)L, \quad (10)$$

where  $c$  is the speed of light in vacuum and  $n_g(\omega_s)$  is the group index at the soliton carrier frequency,  $\omega_s$ . Neglecting changes in  $L$ , the tuning of  $f_{\text{rep}}$  with temperature  $T$  is given by

$$\frac{df_{\text{rep}}}{dT} = \frac{f_{\text{rep}}}{n_g} \frac{dn_g(\omega_s)}{dT}. \quad (11)$$

To remain general, one must include a temperature-sensitive  $\omega_s$  in equation (11), which yields

$$\frac{dn_g}{dT} = \frac{\partial n_g}{\partial T} + \frac{\partial n_g}{\partial \omega_s} \frac{\partial \omega_s}{\partial T}. \quad (12)$$

Equation (12) shows explicitly that the product of dispersion ( $\partial n_g / \partial \omega_s$ ) and soliton-frequency-shift tuning ( $\partial \omega_s / \partial T$ ) affects the total thermo-optic coefficient ( $dn_g/dT$ ), which defines  $\eta_{\text{rep}}$ .

Here we seek to quantify the relative contribution of the soliton frequency shift to  $\eta_{\text{rep}}$ . Instead of  $n_g$ , we work with the more experimentally accessible quantities  $\nu_m$  and  $\Delta$ , and are guided by equation (6). However, both  $\nu_m$  and  $\Delta$  are sensitive to changes in either  $T$  or  $\nu_p$ , so that in the experiment one cannot control

them independently. Therefore, we study the actions of  $\nu_m$ ,  $\Delta$  and  $f_{\text{rep}}$  as a system of equations against controlled changes in  $T$  and  $\nu_p$ . To this end, we measure

$$\frac{df_{\text{rep}}}{d\Delta_T} = \frac{\partial f_{\text{rep}}}{\partial \Delta} + \frac{\partial f_{\text{rep}}}{\partial \nu_m} = 13.5 \text{ MHz GHz}^{-1}, \quad (13)$$

$$\frac{df_{\text{rep}}}{d\Delta_\nu} = \frac{\partial f_{\text{rep}}}{\partial \Delta} + \frac{\partial f_{\text{rep}}}{\partial \nu_m} \frac{\partial \nu_m}{\partial \nu_p} = -25 \text{ MHz GHz}^{-1}, \quad (14)$$

where  $\Delta_T$  implies a temperature-actuated detuning ( $\nu_p$  is fixed) and  $\Delta_\nu$  indicates a pump-frequency-actuated detuning. We can isolate  $\partial f_{\text{rep}}/\partial \nu_m$  and  $\partial f_{\text{rep}}/\partial \Delta$  by subtracting the above equations to cancel out the shared term and get

$$\frac{\partial f_{\text{rep}}}{\partial \nu_m} \left( 1 - \frac{\partial \nu_m}{\partial \nu_p} \right) = 38.5 \text{ MHz GHz}^{-1}. \quad (15)$$

Taking the derivative of  $\nu_m = \nu_p + \Delta$  and using a measured coefficient of  $\partial \nu_p/\partial \Delta = -6.1 \text{ GHz GHz}^{-1}$  gives  $\partial f_{\text{rep}}/\partial \nu_m = 5.2 \text{ MHz GHz}^{-1}$ , and therefore  $\partial f_{\text{rep}}/\partial \Delta = 8.3 \text{ MHz GHz}^{-1}$ . Interestingly, these analyses suggest that understanding the thermal noise in any nonlinear, microresonator-based frequency conversion process requires consideration of both the temperature-dependent refractive index and the detuning-dependent nonlinear processes that are coupled to the temperature.

**Laser cooling and the effective damping rate.** After accessing the soliton state, we apply the cooling laser to the  $\nu_{m+1}$  microresonator mode and counter-propagating with respect to the pump laser and soliton. (The cooling laser is off during soliton generation.) Since the cooling laser induces a static redshift in the mode spectrum, in our experiments we adjust the pump laser to maintain soliton stability and  $f_{\text{ceo}} \approx 1 \text{ GHz}$  during cooling. The pump laser is red-detuned by 3.6 GHz and therefore provides negligible cooling. We characterized this by probing microresonator fluctuations with no soliton present. Interestingly, we have observed that laser cooling is also effective by use of other resonator mode numbers  $m$ , even  $m + 90$ .

In our system, laser cooling plays a substantial role in improving the measurement precision of our soliton microcomb. Indeed, since laser cooling does not modify the average optical power of the soliton, it increases the peak  $f-2f$  photocurrent signal. Such an improvement in signal-to-noise ratio (SNR) has important implications for metrological applications, specifically in higher precision digitization that reduces the  $f_{\text{ceo}}$  detection error rate by a factor  $\propto \text{erfc}(10^{\text{SNR}/20}/\sqrt{2})^{41}$ .

To model soliton laser cooling, we include a photothermal force ( $F_{\text{PT}} = \alpha_T |a|^2$ ) in the Langevin equation according to

$$\frac{d(\delta\nu_{m+1})}{dt} = -\Gamma_T \delta\nu_{m+1} + \alpha_T |a|^2 + \zeta(t). \quad (16)$$

To identify  $\Gamma'$  we expand  $|a|^2$  around  $\delta\nu_{m+1} = 0$ ,

$$|a|^2 = \frac{\kappa_c P_c}{\Delta_c^2 + (\frac{\kappa_{m+1}}{2})^2} = \frac{\kappa_c P_c}{\Delta_c^2 + (\frac{\kappa_{m+1}}{2})^2} + \frac{2\Delta_c \kappa_c P_c}{[\Delta_c^2 + (\frac{\kappa_{m+1}}{2})^2]^2} \delta\nu_{m+1} + \dots \quad (17)$$

The zeroth-order term corresponds to a static shift in  $\nu_{m+1}$  that does not contribute to the photothermal dynamics. Moreover, higher-order terms become increasingly negligible if the  $\nu_{m+1}$  frequency jitter is much less than its linewidth ( $\delta\nu_{m+1} \ll \kappa_{m+1}$ ). We therefore consider only the first-order term, and the Langevin equation becomes

$$\frac{d(\delta\nu_{m+1})}{dt} = -\left( \Gamma_T + \frac{2|\alpha_T| \Delta_c \kappa_c P_c}{[\Delta_c^2 + (\frac{\kappa_{m+1}}{2})^2]^2} \right) \delta\nu_{m+1} + \zeta(t), \quad (18)$$

from which it is clear that  $\Gamma'_T$  is given by the expression in the main text. In the low- $P_c$  limit, which we use as a basic theoretical comparison to our results, the  $f_{\text{ceo}}$  noise reduction can be written<sup>24,29</sup>

$$\langle \delta f_{\text{ceo}}^2 \rangle = \frac{\Gamma_T}{\Gamma'_T} \langle \delta f_{\text{ceo}}^2 \rangle_0. \quad (19)$$

The theory curve in Fig. 4c is derived from this expression with  $\Gamma_T \approx 100 \text{ kHz}$ , which is consistent with measured and predicted resonator thermal time constants, and  $\alpha_T \approx 2 \times 10^{24} \text{ Hz}^2 \text{ J}^{-1}$ , which is estimated from a measurement of the cavity

resonance shift per watt of applied laser power. For higher  $P_c$ , both the absolute intensity and the frequency noise of the cooling laser hinder the cooling efficiency; this behaviour has been reported extensively in laser cooling mechanical systems<sup>42</sup>. A second and more unusual effect of our soliton microcomb system is the initiation of parametric oscillation for  $P_c \geq 20 \text{ mW}$ . Owing to this effect, some of the cooling power is lost to signal and idler generation. We expect that straightforward technical improvements in our system—such as laser cooling with a resonator mode that experiences normal group-velocity dispersion and with a lower-noise laser—should enable experiments to reach  $T_{\text{eff}} < 10 \text{ K}$ .

### Data availability

The data that support the plots within this paper and other findings of this study are available from the corresponding author upon reasonable request.

### References

- Briles, T. C. et al. Interlocking kerr-microresonator frequency combs for microwave to optical synthesis. *Opt. Lett.* **43**, 2933–2936 (2018).
- Stone, J. R. et al. Thermal and nonlinear dissipative-soliton dynamics in Kerr-microresonator frequency combs. *Phys. Rev. Lett.* **121**, 063902 (2018).
- Li, Z. et al. Thulium-doped fiber amplifier for optical communications at 2  $\mu\text{m}$ . *Opt. Express* **21**, 9289–9297 (2013).
- Lamb, E. S. et al. Optical-frequency measurements with a Kerr microcomb and photonic-chip supercontinuum. *Phys. Rev. Appl.* **9**, 024030 (2018).
- Jost, J. D. et al. Counting the cycles of light using a self-referenced optical microresonator. *Optica* **2**, 706–711 (2015).
- Brasch, V., Lucas, E., Jost, J. D., Geiselmann, M. & Kippenberg, T. J. Self-referenced photonic chip soliton Kerr frequency comb. *Light Sci. Appl.* **6**, e16202 (2017).
- DiDomenico, G., Schilt, S. & Thomann, P. Simple approach to the relation between laser frequency noise and laser line shape. *Appl. Opt.* **49**, 4801–4807 (2010).
- Huszank, R., Csedreki, L., Kertész, Z. & Török, Z. Determination of the density of silicon-nitride thin films by ion-beam analytical techniques (RBS, PIXE, STIM). *J. Radioanalyt. Nucl. Chem.* **307**, 341–346 (2016).
- Bai, S., Tang, Z., Huang, Z. & Yu, J. Thermal characterization of  $\text{Si}_3\text{N}_4$  thin films using transient thermoreflectance technique. *IEEE Trans. Ind. Electr.* **56**, 3238–3243 (2009).
- Li, Q. et al. Stably accessing octave-spanning microresonator frequency combs in the soliton regime. *Optica* **4**, 193–203 (2017).
- Xue, X. et al. Thermal tuning of Kerr frequency combs in silicon nitride microring resonators. *Opt. Express* **24**, 687–698 (2016).
- Sinclair, L. C. et al. A compact optically coherent fiber frequency comb. *Rev. Sci. Instrum.* **86**, 081301 (2015).
- Kippenberg, T. J., Schliesser, A. & Gorodetsky, M. Phase noise measurement of external cavity diode lasers and implications for optomechanical sideband cooling of ghz mechanical modes. *N. J. Phys.* **15**, 015019 (2013).

### Acknowledgements

We thank K. Srinivasan for fabricating the SiN microresonators, S.-P. Yu for creating the mode simulation in Fig. 1, D. Spencer for experimental assistance, and Srico, Inc. for the use of the periodically poled lithium-niobate waveguide device. This research is supported by the Defense Advanced Research Projects Agency DODOS programme, AFOSR (FA9550-16-1-0016), NRC and NIST.

### Author contributions

T.E.D. and J.R.S. performed the experiments and analysed the data. T.C.B. assisted in all aspects of the work. S.B.P. contributed to all aspects of the work and supervised the project.

### Competing interests

The authors declare no competing interests.

### Additional information

Supplementary information is available for this paper at <https://doi.org/10.1038/s41566-020-0651-8>.

Correspondence and requests for materials should be addressed to S.B.P.

Reprints and permissions information is available at [www.nature.com/reprints](http://www.nature.com/reprints).